Heliyon 10 (2024) e25761

Contents lists available at ScienceDirect

Heliyon

journal homepage: www.cell.com/heliyon

Research article

Quantification of surface-localized and total oxytocin receptor in myometrial smooth muscle cells

Yingye Fang [a], Erin L. Reinl [b], Audrey Liu [b], Trinidi D. Prochaska [b], Manasi Malik [b], Antonina I. Frolova [b], Sarah K. England [b], Princess I. Imoukhuede [a,*]

[a] Department of Bioengineering, University of Washington, Seattle, WA, 98109, USA
[b] Department of Obstetrics and Gynecology, Center for Reproductive Health Sciences, Washington University School of Medicine in St. Louis, St. Louis, MO, 63110, USA

ARTICLE INFO

Keywords:
Oxytocin receptor
Quantitative flow cytometry
Protein surface localization
Genetic variants

ABSTRACT

Oxytocin acts through the oxytocin receptor (OXTR) to modulate uterine contractility. We previously identified OXTR genetic variants and showed that, in HEK293T cells, two of the OXTR protein variants localized to the cell surface less than wild-type OXTR. Here, we sought to measure OXTR in the more native human myometrial smooth muscle cell (HMSMC) line on both the cell-surface and across the whole cell, and used CRISPR editing to add an HA tag to the endogenous OXTR gene for anti-HA measurement. Quantitative flow cytometry revealed that these cells possessed 55,000 ± 3200 total OXTRs and 4900 ± 390 cell-surface OXTRs per cell. To identify any differential wild-type versus variant localization, we transiently transfected HMSMCs to exogenously express wild-type or variant OXTR with HA and green fluorescent protein tags. Total protein expression of wild-type OXTR and all tested variants were similar. However, the two variants with lower surface localization in HEK293T cells also presented lower surface localization in HMSMCs. Overall, we confirm the differential surface localization of variant OXTR in a more native cell type, and further demonstrate that the quantitative flow cytometry technique is adaptable to whole-cell measurements.

1. Motivation

Clinical response to synthetic forms of oxytocin varies widely across individuals. In some cases, this may be due to the low abundance of the oxytocin receptor (OXTR) on the cell surface. However, no OXTR-specific antibodies are available to quantify surface and total OXTR. To address this challenge, we developed a flow cytometry method to quantify OXTR in human myometrial smooth muscle cells. Furthermore, quantitative flow cytometry is extensively used to measure receptors on the cell surface, but the cell-surface compartment only offers limited insight into receptor trafficking regulation, which can be further advanced through whole-cell measurements. To advance insight into receptor compartmentalization, here we conduct both cell surface and whole-cell OXTR measurements.

* Corresponding author.
E-mail address: pii@uw.edu (P.I. Imoukhuede).

https://doi.org/10.1016/j.heliyon.2024.e25761
Received 18 October 2023; Received in revised form 31 January 2024; Accepted 1 February 2024
Available online 13 February 2024

2. Introduction

Oxytocin regulates social behavior, reproductive function, and lactation by signaling via its G-protein-coupled oxytocin receptor (OXTR). Synthetic oxytocin (Pitocin) is commonly administered to induce and strengthen uterine contractions in labor and to prevent postpartum hemorrhage, and it is a potential therapy for multiple neuropsychiatric disorders [1]. However, the oxytocin response varies widely across individuals. For example, for labor induction and augmentation, oxytocin doses range from 1 to 40 milliunits per minute and are titrated every 15–60 min [2]. Improper dosing can result in adverse outcomes such as fetal distress and uterine rupture [3]. Personalizing oxytocin dosage based on individual differences in oxytocin sensitivity could improve the safety and effectiveness of treatment.

Cell response to oxytocin is influenced by OXTR availability. At the onset of term labor, uterine OXTR protein expression increases to be around 20 times higher than in mid-gestation states and 100 times higher than in non-pregnant states [4]. In *in vitro* experiments, oxytocin-responsive myometrial tissue exhibits approximately 10-fold higher OXTR protein expression than oxytocin-nonresponsive tissue [5]. Two hypothetical explanations for the decreased OXTR availability in oxytocin-nonresponsive individuals are genetic variation [6] and hormone dysregulation [7]. To devise personalized oxytocin dosage, we need a strategy to quantify OXTR surface localization and total protein expression. However, we currently lack OXTR-specific antibodies, as those available may also bind the structurally similar vasopressin receptors [8,9]. Thus, new measurement approaches are needed.

One way to overcome these challenges is to add an epitope tag such as HA, FLAG, or His to the extracellular, N-terminal region of OXTR. CRISPR editing [10] can be used to modify the endogenous OXTR gene, alternatively, stable or transient cell transfection can be used for exogenous expression of tagged OXTR [10,11]. Transient cell transfection is the easiest, quickest, and most cost-effective approach but typically results in a large population of non-transfected cells. These tag-negative cells can skew OXTR measurements in bulk protein analysis. By adding a GFP tag to the intracellular, C-terminal end of the OXTR, we can readily select GFP-positive transfected cells for single-cell protein analysis by flow cytometry. While conventional flow cytometry generates relative fluorescence intensities, which would enable detection of these HA and GFP-tagged OXTR + cells, these data are only semi-quantitative. Thus, this method has limited utility in consolidating and comparing results across experiments conducted with different variants, on different days, or by different research groups. The absence of precise quantitative measurements for OXTR hampers the establishment

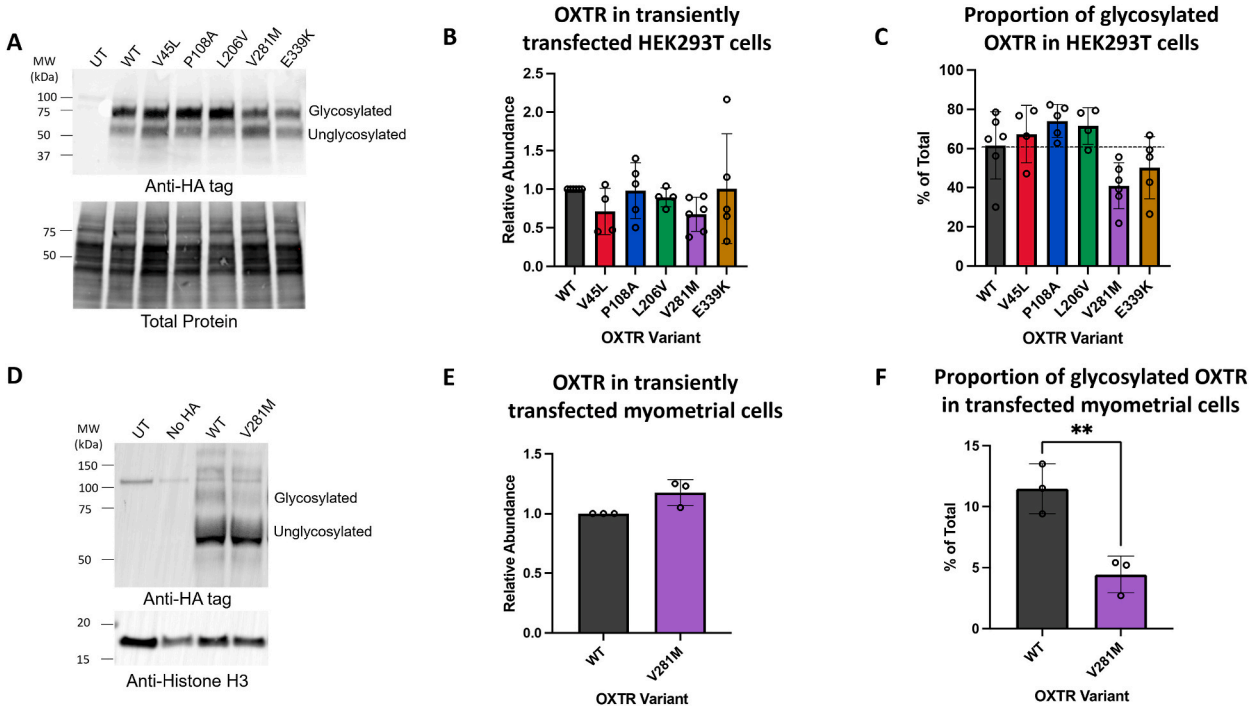

Fig. 1. Western blotting to measure OXTR expression in HEK293T cells and HMSMCs. (A) Representative HA western blot (upper) and total protein staining (lower) of un-transfected (UT) HEK293T cells or HEK293T cells transfected with constructs expressing wild-type (WT) OXTR or the indicated variants. (B) Quantification of total OXTR expression, normalized to total protein and then to the WT sample. No significant differences were found by Kruskal-Wallis ANOVA. (C) The percentage of OXTR variants that are glycosylated is calculated by dividing the intensity of the upper band by the sum of both bands. $P = 0.003$ by one-way ANOVA. (D) Representative HA western blot (upper) and histone H3 western Blot (lower) of UT hTERT-HM cells or hTERT-HM cells transfected with constructs expressing OXTR-GFP, WT OXTR, or V281 M OXTR. (E) Quantification of total OXTR expression, normalized to histone H3 and then to the WT sample. No significant differences were observed by the Wilcoxon Signed-Rank test. (F) The percentage of OXTR variants that are glycosylated is calculated by dividing the intensity of the upper band by the sum of both bands. **$P < 0.01$ by paired *t*-test. Uncropped western blots are shown in Supplementary Fig. 1 (A and B).

of a standardized biomarker for guiding effective oxytocin use clinically.

We previously used quantitative flow cytometry (qFlow) to quantify exogenous OXTR in HEK293T cells [11]. We measured surface localization and total expression of wild-type OXTR and five genetic variants of the OXTR. Total protein expression was similar for wild-type OXTR and all five variants. However, the OXTR variants P108A and L206V localized to the cell surface significantly more than wild-type OXTR (23 ± 3% and 41 ± 4%, respectively, more; $p < 0.05$). Conversely, the OXTR variants V281 M and E339K localized to the cell surface significantly less than wild-type OXTR (49 ± 0.7% and 36 ± 2%, respectively, less; $p < 0.05$) [11]. Our fluorescence imaging results revealed increased Golgi localization of V281 M and E339K, suggesting a defect in OXTR trafficking [10]. Moreover, assessment of Ca^{2+} release and β-arrestin recruitment indicated that HEK293T cells expressing V281M-OXTR had less OXTR signaling than HEK293T cells expressing wild-type OXTR [11]. In subsequent work, we identified chaperone drugs that restored the surface localization of V281 M OXTR [10].

An important challenge of the previous work was that OXTR was expressed in HEK293T cells, which do not express endogenous OXTR and thus likely lack important machinery for OXTR trafficking and signaling. Thus, here, we optimized the qFlow method to measure OXTR localization on the cell surface and across the whole cell in human myometrial smooth muscle cells (HMSMCs). In addition to the insights we achieve in the more native cell, this novel protocol can be applied to quantify OXTR total and cell surface abundance in other cell types and to quantify other transmembrane proteins on the cell surface and across the whole cell.

3. Results

3.1. Western blotting confirms that OXTR variants differ in surface localization but not in total expression in HEK293T and myometrial muscle cells

In our previous qFlow experiments, the total concentrations of wild-type OXTR and five variants were similar in HEK293T cells [11]. To confirm this finding, we performed western blots of lysates from HEK293T cells transiently transfected with constructs in which wild-type or variant OXTR proteins were tagged with HA on the N-terminus. All lanes contained two bands when probed with anti-HA antibody (Fig. 1A). When we treated the cell lysates with peptide: N-glycosidase F before western blotting, only the lower band appeared (data not shown), indicating that the lower band was unglycosylated OXTR, and the upper band was a glycosylated form of the receptor. Glycosylation is a post-translational modification that regulates the trafficking of many G protein-coupled receptors to the cell surface [12]. We quantified the intensities of both bands and normalized them to total protein. Total expression (sum of the two bands) did not significantly differ between wild-type OXTR and the five variants (Fig. 1B). The upper bands were weaker in cells expressing V281 M and E339K, suggesting less glycosylation ($P = 0.003$) (Fig. 1C).

Additionally, our western blot data indicates that the glycosylation of OXTRs on the cell surface does not mask the HA tag, because the abundance of glycosylated OXTRs mirrors the surface-localized OXTR levels measured by qFlow (Fig. 1C). The western blot measurements of glycosylated OXTRs further align with our previously published qFlow measurements of HEK293T cells transfected with OXTR variants (Fig. 1A): compared to wild-type receptors, V45L had similar surface levels, P108A and L206V had more surface receptors, and V281 M and E339K had fewer surface receptors [11].

To determine whether OXTR distribution was regulated similarly in the more native HMSMCs as in the prior studied HEK293T cells, we transiently transfected immortalized HMSMC cells with constructs to express wild-type or variant OXTR with an N-terminal HA tag and a C-terminal GFP tag. We then sorted the cells based on their GFP expression and analyzed the GFP-positive cells by western blot with an anti-HA antibody (Fig. 1D). Total expression of wild-type and V281 M OXTR was similar (Fig. 1E), but the proportion of receptors that were glycosylated was 62% lower for V281 M than for wild-type OXTR ($P = 0.009$) (Fig. 1F). This aligns with the idea that post-translational processing or trafficking of V281 M OXTR is impaired [11].

3.2. qFlow quantifies endogenous OXTR distribution in myometrial muscle cells

We next wanted to determine how many OXTR molecules are expressed and localized to the cell surface when expressed from the

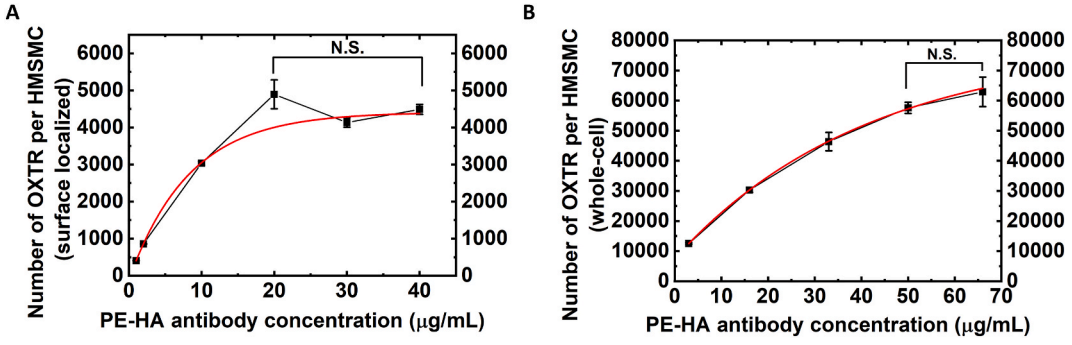

Fig. 2. Determination of saturating PE-HA antibody concentrations. Titration curves of PE-HA antibody concentrations for (A) cell surface and (B) total expression.

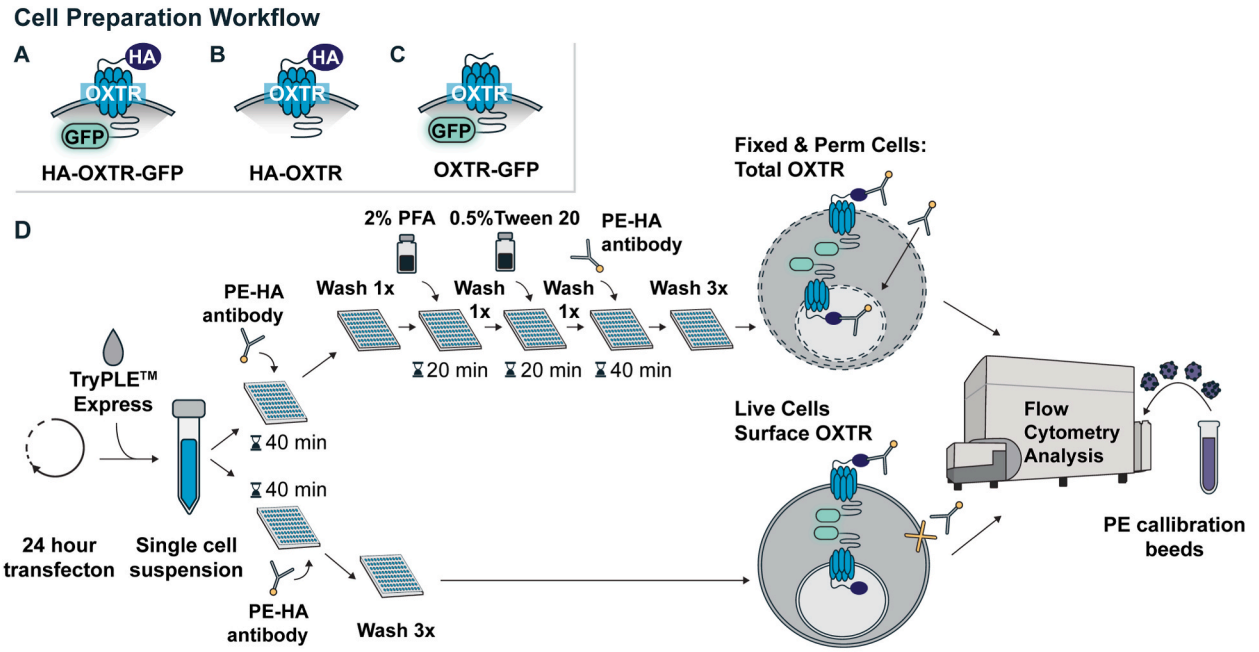

Flow Cytometry Gating Steps

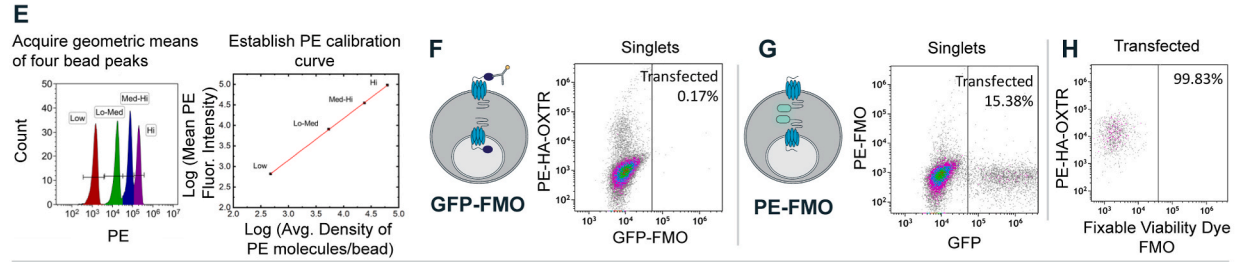

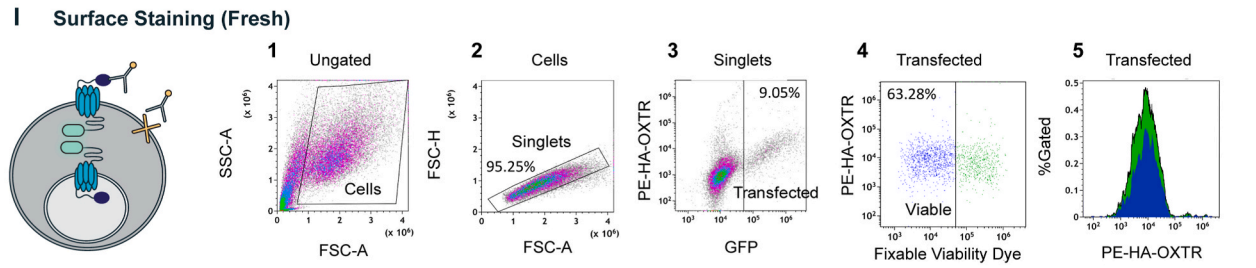

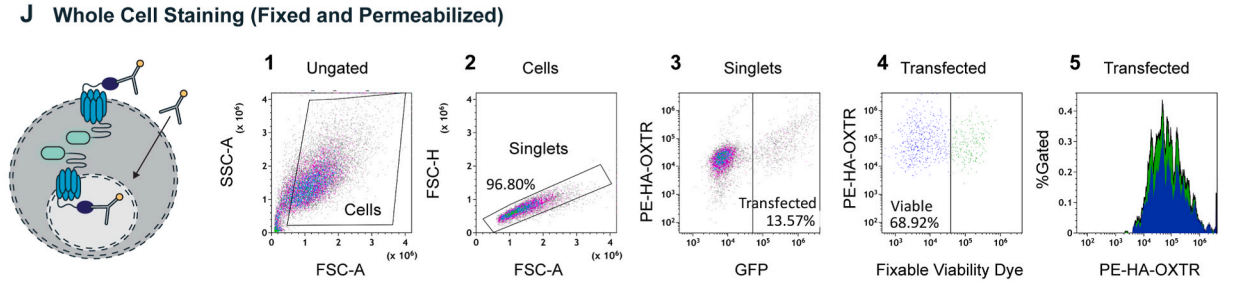

(caption on next page)

Fig. 3. Flow cytometric analysis of OXTR total expression and surface localization in HMSMCs. (A–C) Schematic illustrating the (A) wild-type and variant HA-OXTR-GFP constructs and the (B, C) HA-OXTR and OXTR-GFP constructs. (D) Procedure for labeling intracellular and surface-localized OXTR with PE-conjugated anti-HA antibody and eFluor 780-conjugated fixable viability dye (FVD). (E) Calibration curve converting PE fluorescence intensity to PE molecule counts. (F, G) GFP-fluorescence-minus-one (FMO) and PE-FMO signal cutoffs in HA-OXTR and OXTR-GFP transfected cells, respectively. (H) FVD-FMO signal cutoff for determining cell viability. (I–J) Selection criteria for flow cytometric data acquisition of HA-OXTR-expressing cells based on scatter properties (non-debris and singlets), GFP^+ transfection, and FVD^- viability status.

endogenous locus in immortalized HMSMCs. Firstly, we used CRISPR to add an HA tag to the N-terminus of the OXTR gene. Secondly, we identified the antibody concentration needed to label all of the total and cell-surface HA-OXTR molecules by performing a saturation study (Fig. 2A and B), titrating phycoerythrin (PE)-conjugated anti-HA antibody. We chose the PE-conjugated anti-HA antibody because PE antibody has a fluorophore/protein ratio of 1.0, whereas other fluorophores (e.g., FITC and APC) are conjugated to antibodies at varying ratios [13]. Thirdly, we used Quantibrite PE calibration beads to create a calibration curve for the PE fluorescent signal, as previously described [13]. At saturating concentrations of PE-conjugated anti-HA antibody (20 μg/mL for cell surface OXTR and 50 μg/mL for whole-cell OXTR), CRISPR-edited HMSMCs contained 4900 cell-surface OXTRs (Fig. 2A), 55 and 000 total OXTRs per cell (Fig. 2B). Ultimately, we observed ~9% of endogenous wild-type OXTRs were localized at the cell surface and 91% were intracellular.

3.3. *qFlow quantifies exogenous OXTR variants in myometrial muscle cells*

Next, we transiently transfected HMSMCs with constructs expressing wild-type OXTR or each of the five variant OXTRs, all tagged with HA on the N-terminus and GFP on the C-terminus (Fig. 3A). Additionally, we generated cells expressing HA-OXTR or OXTR-GFP (Fig. 3B and C) to serve as fluorescence-minus-one (FMO) controls for multi-color flow cytometry analysis, as described in the STAR Methods.

To quantify OXTR protein expression on the cell surface, we prepared a single-cell suspension [13] and incubated the cells with saturating PE-conjugated anti-HA antibody and eFluor 780–conjugated fixable viability dye (FVD). To quantify total OXTR protein expression, we fixed and permeabilized the PE-labeled cells and incubated them again with PE-HA antibody to label the intracellular HA-OXTR (Fig. 3D). The numbers of HA-OXTR molecules per cell were calculated using the PE calibration curve (Fig. 3E). OXTR–GFP–transfected cells served as a PE-FMO control, in which the PE signal came from cell autofluorescence and non-specific PE antibody binding to the cells (Fig. 3C and G). We subtracted this PE-FMO signal from the PE-HA signals to obtain a background-free PE signal. HA-OXTR-transfected cells served as a GFP-FMO control to determine the GFP^+/GFP^- signal cutoff (Fig. 3B and F). Similarly, the FVD-FMO control was used to determine the FVD^+/FVD^- cutoff (Fig. 3H). During flow cytometric data acquisition, HA-OXTR-expressing cells were selected according to the following properties for surface OXTR (Fig. 3I) and whole-cell OXTR

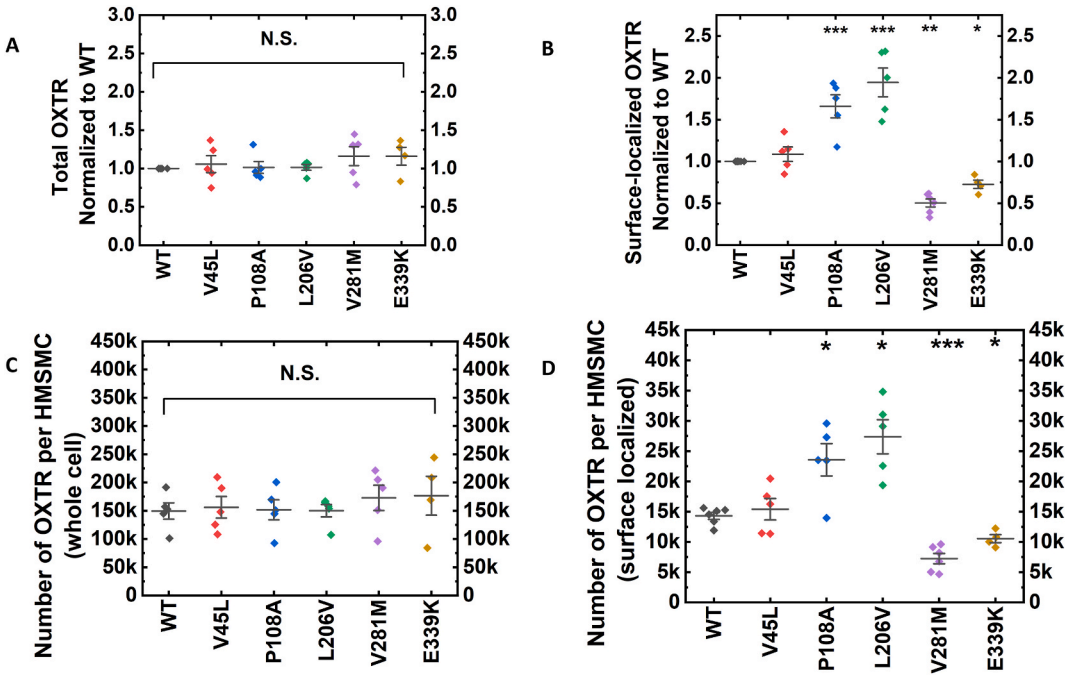

Fig. 4. Total expression and surface localization of OXTR variants in transiently transfected HMSMCs. (A, B) Relative total (A) and surface-localized (B) wild-type and variant OXTR in MSMCs. (C, D) The absolute number of total (C) and surface-localized (D) wild-type and variant OXTR molecules per HMSMC. *P < 0.05, **P < 0.01, ***P < 0.001, ****P < 0.0001 by Two-sample *t*-test.

quantification (Fig. 3J): (1) non-debris cells (SSC vs. FSC); (2) singlets (FSC–H vs. FSC-A): (3) transfected (GFP^+); and (4) viable during the surface-labeling step (FVD^-).

We compared the total expression and surface localization of wild-type OXTR and the five variants in transiently transfected HMSMCs. All of the OXTR variants had a similar total expression as wild-type OXTR (Fig. 4A and C). However, compared to wild-type OXTR, we measured 65.9 ± 13.8% more P108A OXTR ($p < 0.05$) and 94.5 ± 17.1% more L206V OXTR ($p < 0.05$) on the cell surface. Conversely, 49.8 ± 4.8% less V281 M OXTR ($p < 0.05$) and 28.4 ± 4.9% less E339K OXTR ($p < 0.05$) were on the cell surface. The amount of V45L OXTR on the cell surface was similar to that of wild-type OXTR (Fig. 4B and D). The directionality of the differences in surface and total OXTR expression between wild type and variants were similar to what we observed in HEK293T cells [11], despite variations in the magnitudes of effects and the surface-to-total OXTR ratios.

Finally, although transfected HMSMCs expressed three-fold more OXTR molecules than HMSMCs endogenously expressing OXTR, the percentage of OXTR on the cell surface was similar (9.9% and 8.9%, respectively) (Table 1). The surface localization of approximately 10% total OXTR also closely matches the glycosylation rate measured by western blot, further validating our qFlow findings (Fig. 1C). In contrast to the transfected HMSMCs, 20.9% of OXTRs were on the surface of transfected HEK293T cells. We conclude that the transfected HMSMCs more closely recapitulate endogenous OXTR expression and trafficking in HMSMCs than do transfected HEK293T cells.

4. Discussion

We optimized qFlow to measure the surface localization and total protein expression of OXTR in human myometrial smooth muscle cells (HMSMCs). Our qFlow data indicate that the five OXTR variants studied are expressed at similar amounts as wild-type OXTR in HMSMCs, but different proportions localize to the cell surface. These data align with our previous observations in HEK293T cells [11]. Additionally, the novel whole-cell qFlow approach provides biologically accurate insights into the spatial regulation of OXTR, such as OXTR surface localization, in transfected myometrial cells. Our findings indicate that the WT OXTR surface localization rate is ~10% of the total OXTR protein in both transfected myometrial cells and CRISPR-edited (endogenous) myometrial cells, suggesting the endogenous OXTR surface localization rate is preserved in the transfected myometrial cells. In HEK293T cells, transfected WT OXTRs exhibited higher surface localization than in the myometrial cells at ~20% surface localization. This higher OXTR surface localization in HEK293T cells may be attributed to either the absence of native OXTR internalization machinery or the overexpression of the plasmid construct in these cells. Although the transfected HEK293T cells are useful for assessing expression and cell surface localization of OXTR variants, the transfected HMSMCs are more biologically relevant for studies of OXTR trafficking in the myometrium.

Our qFlow data on OXTR surface localization and total expression in HMSMCs could lead to personalized oxytocin dosing strategies to improve uterine contraction. We previously tested the oxytocin dose response for inducing OXTR activation (i.e., IP1 production) in transfected HA-OXTR HEK293T cells, CRISPR-edited HA-OXTR HMSMCs, and primary HMSMCs from patients [10]. We observed that the HA-tagged HEK293T cells and the HA-tagged HMSMCs reached the maximal IP1 accumulation level at similar oxytocin doses, despite the HA-tagged HEK293T cells displaying ten times more surface OXTRs and five times more total OXTRs than the HA-tagged HMSMCs [10], suggesting that OXTR overexpression does not result in saturation of the oxytocin signaling pathway. Additionally, we observed that the HA-tagged HMSMCs had higher maximal responses to oxytocin after being pre-treated with pharmacological chaperones, which increased the surface OXTR level before the oxytocin treatment [10]. The same chaperone effects were observed in the primary HMSMCs from patients [10], suggesting the HA-tagged HMSMCs could be a reliable model for predicting oxytocin responses in primary cells. For the ~0.4% pregnant population carrying these OXTR variants (Table 2), our approach can facilitate personalized oxytocin dosing to enhance the effectiveness of labor induction or prevent postpartum hemorrhage. Extending beyond genetic variants, our approach holds significant potential to experimentally address the mechanisms behind other risk factors for reduced oxytocin sensitivity, including obesity, type II diabetes, or prolonged exposure to oxytocin during labor induction [14,15]. Lastly, the qFlow approach can also be used to evaluate the effects of candidate therapeutics that increase OXTR cell surface availability [10]. Such therapeutics could be used to optimize labor induction or augmentation.

Potential interventions and future personalized dosing of oxytocin may be guided by data-driven computational models that recapitulate OXTR trafficking and signaling. Our receptor measurements are important parameters for such models, which rely heavily on quantitative data to predict cell and system function. For example, previous data-driven computational models provided mechanistic insights into how the abundance of receptor tyrosine kinases (e.g., VEGFRs) impacts resistance to anti-angiogenic drugs [16–18]. Similarly, the OXTR measurements can be used in computational models to help personalize oxytocin dosages or devise therapy for individuals with OXTR genetic variants.

Compared with the current gold standard assays for cell-surface protein measurements, such as western blotting and traditional flow cytometry, qFlow is a more quantitative tool for analyzing cell-surface and intracellular proteins. We previously used this approach to study cell-surface-bound receptors, such as receptor tyrosine kinases and G-protein–coupled receptors [13]. The

Table 1
Quantification of surface and total OXTR expression.

Wild Type OXTR	CRISPR-edited HMSMC (endogenous)	Transfected HMSMC	Transfected HEK293T[9]
Cell Surface (# OXTRs/cell)	4900 ± 390	14,300 ± 574	160,000 ± 22,200
Total OXTR (# OXTRs/cell)	55,000 ± 3200	145,000 ± 14,460	767,000 ± 55,000
Percent OXTR on the cell surface	8.9%	9.9%	20.9%

Table 2
Missense variants in OXTR in this study (gnomAD v4.0 data).

Variant	dbSNP	Frequency (%) in Total Population (gnomAD v4.0)	*Most Affected Population**
L206V	rs150746704	0.11	African/African America
E339K	rs143927655	0.13	Ashkenazi Jewish
V281 M	rs144814761	0.05	European (non-Finnish)
V45L	rs202094106	0.07	European (non-Finnish)
P108A	rs202138705	0.02	European (Finnish)

quantitative single-cell receptor tyrosine kinase data revealed heterogeneity in tumor and tumor-associated vascular cells [19–21], vessel-like tubules [22], and normal vascular cells [23–26]. The high-resolution single-cell protein data have been used to advance computational modeling [27–32]. Given its versatility and reproducibility, our method can be easily adapted to quantify OXTR abundance in numerous cell types given the role of OXTR in health and disease [33], such as neurons (relevant to autism [34] and neurodegenerative disease research [35]), myoepithelial cells (relevant to lactation [36] and breast tumors [37]), and specialized colon cells (relevant to gut microbiome studies [37]). Furthermore, our protocol can be adapted to measure different OXTR variants, other cell-surface-bound receptors, and diverse cell types to gain insights into receptor trafficking mechanisms involved in various physiological and pathological processes.

5. Future opportunities

The qFlow-based approach used in this study has two important challenges. First, the ability to better differentiate intracellular compartments would enable additional insight into OXTR compartmentalization This challenge can be addressed by coupling fluorescence imaging of OXTR trafficking to qFlow [10]. Second, given the lack of commercially available, OXTR-specific antibodies, we applied an innovative approach to genetic modification of the OXTR gene to incorporate an HA tag that can be detected by PE-HA antibodies. We used two approaches to introduce the HA tag. Transfection of plasmids encoding HA-OXTR allowed us to compare OXTR variants in the same cell type. CRISPR modification to introduce an N-terminal HA tag to the endogenous OXTR gene allowed us to measure endogenous OXTR expression. However, in both cases, the effect of the HA tag on OXTR trafficking and function is unknown. The development of OXTR-specific affinity probes would obviate the need for protein tagging. Once such reagents are developed, the qFlow method we present here could be used to quantify OXTR in any cell type, including freshly isolated cells from human tissues.

6. STAR methods

6.1. Key resources table

Reagent or Resources	Source	Identifier
Cell lines		
HEK293T	ATCC	CRL-3216
hTERT-HM human myometrial smooth muscle cells	Jennifer Condon	N/A
CRISPR-edited hTERT-HM cells with OXTR-HA	The Genome Engineering and iPSC Center at Washington University in St. Louis	N/A
Chemicals, proteins, transfection materials		
Lipofectamine™ 3000	Invitrogen	L3000015
DMEM/F-12, no phenol red	Gibco	21041025
TryPLE™ Express, no phenol red	Gibco	12604013
0.25% Trypsin, phenol red	Gibco	25200056
Opti-MEM	Gibco	31985070
Tween-20	Sigma	P9416
Paraformaldehyde	Sigma	P6148
DPBS	Gibco	14190–136
Bovine Serum Albumin	Fisher	BP9703
Fetal Bovine Serum	Gibco	16000044
PE-conjugated anti-HA1.1 antibody	Biolegend	901518
PE Phycoerythrin Fluorescence Quantitation Kit	BD Biosciences	340495
Fixable Viability Dye eFluor™ 780	eBioscience™	65-0865-14
Cytometer QC Beads	Cytek® Biosciences	B7-10001
Hanks Buffered Saline Solution	Gibco	14025–076
RIPA lysis buffer	Sigma	R0278
Halt Protease and Phosphatase Inhibitors	Thermo Scientific	1861281
0.1 mm Glass Beads	Stellar Scientific	GB01
Bicinchoninic Acid Assay	Pierce, Thermo Scientific	23223, 23224
Bolt LDS Sample Buffer	Novex, Thermo Fisher Scientific	B0008
0.45 μm Nitrocellulose	Bio-Rad	1620115

(*continued on next page*)

(*continued*)

Reagent or Resources	Source	Identifier
Tris/Glycine/SDS Buffer	Bio-Rad	1610732
Tris/Glycine Buffer	Bio-Rad	1610734
Mini-PROTEAN TGX Precast Protein Gels	Bio-Rad	4561021
Revert 700 Total Protein Stain	Li-Cor	926–11011
Rabbit anti-HA antibody	Cell Signaling Technology	C29F4
Anti-rabbit IgG, HRP-linked Antibody	Cell Signaling Technology	70745
SuperSignal West Femto Maximum Sensitivity Substrate	Thermo Fisher Scientific	34096
Immobilon-P Transfer Membrane, PVDF, 0.45 μm	Millipore Sigma	IPVH00005
Bolt™ 4–12% Bis-Tris Plus	Invitrogen	NW04120BOX
Bolt™ Transfer Buffer (20x)	Invitrogen	BT00061
Bolt™ MES SDS Running Buffer (20x)	Invitrogen	B0002
Anti-Histone H3	Abcam	ab1791
Hoescht 33342	Invitrogen	H3570
Software		
Kaluza flow cytometry analysis software	Beckman Coulter	
OriginLab Pro	OriginLab Corporation	
Image Lab	Bio-Rad	v 6.1.0
GraphPad Prism	GraphPad Software, LLC	v 9.5.1
Instrument		
Cytek® Aurora	Cytek® Biosciences	4L V16–B14-YG10-R8
BD FACSAriaII	BD Biosciences	
Countess® II Automated Cell Counter	Life Technologies	AMQAX1000
Countess™ Cell Counting Chamber Slides	Life Technologies	C10283
Bullet Blender	Stellar Scientific	
ChemiDoc MP Imaging System	Bio-Rad	

Resource availability

Lead contact: Princess Imoukhuede, pii@uw.edu.

Material Availability: All materials and constructs used in this study are maintained by Dr. Imoukhuede's and Dr. England's laboratories and are available upon request.

Data availability: The main data supporting the results of this study are available within the paper. The raw and analyzed datasets are available for research purposes from the corresponding authors upon reasonable request.

7. Experimental model and subject details

Cell lines: HEK293T, hTERT-HM, CRISPR-HM.

Plasmids: Plasmids encoding HA-OXTR, OXTR-GFP, HA-OXTR-GFP, and the OXTR variants were described previously [11].

CRISPR editing and validation: The CRISPR editing was performed using homology-directed repair with the guide RNA sequence GCTGCCGCCAGGGTCATGGANGG at the Genome Engineering & iPSC Center at Washington University in St. Louis. The cell line was monoclonal hTERT-immortalized human uterine smooth muscle cells (clone 8F10). These CRISPR-edited hTERT myometrial cells were engineered to include an HA tag in the sequence of the antisense oligomer. To ensure specificity and to rule out off-target effects, we sequenced the entire OXTR gene in the CRISPR-edited hTERT myometrial cells, confirming the absence of any other missense SNPs/SNVs.

7.1. Method details

7.1.1. Cell transfection

hTERT-HM cells (provided by Jennifer Condon [38]) and HEK293T cells were maintained in DMEM F-12 media supplemented with 10% fetal bovine serum and 25 μg/mL gentamicin.

hTERT-HM cells were treated with 0.25% Trypsin EDTA (Gibco) and counted on a Countess II cell counter (Thermo Fisher). Then, 250,000 cells were plated in 1.5 mL of medium in one well of a 6-well plate. They were immediately transfected according to the manufacturer's protocol (Invitrogen) with 6 μg of the designated plasmids, 7.5 μL Lipofectamine 3000, and 5 μL P3000 in a total of 250 μL OptiMEM.

HEK293T cells were treated with 0.05% Trypsin EDTA (Gibco) and split into 10 cm dishes at ~70% confluence. They were immediately transfected according to the manufacturer's protocol (Mirus) with 540 ng of the designated plasmids and 7.2 μL TransIT LT1 in 600 μL of OptiMEM.

The transfection introduced one of the six OXTR types to the hTERT-HM or HEK293T cells: wild type, L206V, E339K, V281 M, V45L, and P108A. The dbSNP ID, frequency in the total population, and the most affected population of the genetic variants are shown

in Table 2.

7.1.2. Cell dissociation and preparation

Cells were detached 24 h after transfection by incubating with TrypLE Express Enzyme (no phenol red, Gibco) for 8 min at 37 °C. Cells were then collected by centrifugation at 400×*g* for 5 min at 4 °C. Cells were resuspended in staining buffer (0.5% BSA and 0.1% sodium azide in Ca^{2+}/Mg^{2+}-free DPBS, pH 7.4) at ~10^6 cells/mL, and 80 μL of cell suspension was transferred to one well of a round-bottom 96-well plate in triplicate or quadruplicate.

7.1.3. Cell-surface and whole-cell HA-OXTR staining

The optimal concentrations of PE-conjugated HA antibodies for cell-surface and whole-cell HA labeling were determined by a saturation study [23,25]. For cell-surface HA labeling, a saturating concentration of PE-conjugated HA antibodies (20 μg/mL PE-HA, Biolegend) was added to each sample well. For cell viability staining, 1:5000 Fixable Viability Dye (FVD) eFluor 780 (eBioscience) was added to each sample well. FVD eFluor 780 was diluted to 1:500 in DPBS before adding to the sample wells. Therefore, each sample well contained 80 μL single-cell suspension, 10 μL PE-HA antibody, and 10 μL FVD eFluor 780. Cells were incubated in the dark at 4 °C for 40 min and then washed three times with cold staining buffer. After each wash, cells were centrifuged at 400×*g* for 5 min at 4 °C. Cells were resuspended in 100 μL staining buffer and ready for flow cytometry analysis.

For whole-cell HA labeling, cells that had been labeled for cell-surface HA was resuspended in 100 μL of 2% paraformaldehyde (prewarmed to slightly above room temperature), mixed thoroughly by pipetting, and incubated in the dark for 20 min at room temperature. The fixed cells were then washed once with room-temperature DPBS and centrifuged at 400×*g* for 5 min at 23 °C. The washed fixed cell samples were resuspended in 100 μL permeabilization buffer (0.5% Tween 20 in DPBS), mixed thoroughly by pipetting and incubated in the dark for 20 min at room temperature. The fixed and permeabilized cells were then washed once with 0.1% Tween 20 in staining buffer (room temperature) by centrifugation at 400×*g* for 5 min at 23 °C.

The saturating concentration of PE-conjugated HA antibodies that had been experimentally determined for whole-cell staining (50 μg/mL PE-HA, Biolegend) was prepared in 0.1% Tween 20 staining buffer (e.g., 10 μL antibody + 30 μL buffer). The washed, fixed, and permeabilized cell samples were resuspended in the PE-containing staining buffer mixed well by pipetting, and incubated in the dark for 40 min at room temperature. Cells were then washed three times with room-temperature 0.1% Tween 20 staining buffer. After each wash, they were centrifuged at 400×*g* for 5 min at 23 °C. The washed cells were resuspended in 50 μL staining buffer (~50% cell loss was observed after several washes during fixation, permeabilization, and whole-cell staining) and ready for flow cytometry analysis.

7.1.4. Flow cytometry signal calibration, acquisition, and cell selection

Before analyzing cells in the flow cytometer, PE signals of BD Quantibrite PE beads were recorded at the same instrument settings (i.e., PE voltage) as the assay. BD Quantibrite PE beads are used to convert PE signal intensity into the number of PE molecules bound per cell. Quantibrite PE beads comprise a combination of polystyrene beads conjugated with different densities of PE molecules: low (474 PE molecules/bead), medium-low (5,359 PE molecules/bead), medium-high (23,843 PE molecules/bead), and high (62,336 PE molecules/bead).

Flow cytometric data analysis was performed in Kaluza analytical software (Beckman Coulter). To select the cells of interest, which were viable single cells transfected with HA-OXTR-GFP, the following steps were performed: (1) an FSC-Area vs. SSC-Area plot was used to select non-debris cells; (2) an FSC-Height vs. FSC-Area plot (or preferably FSC-Height vs. FSC-Width if available) was used to select single cells; (3) a PE vs. GFP plot was used to select transfected (all GFP^+) cells; and (4) an FSC-Area vs. FVD eFluor 780 plot was used to select viable (FVD^-) cells. PE signals of viable GFP^+ single cells were plotted against cell frequency in a histogram and exported as geometric mean PE values. Geometric mean values of PE intensities of individual samples and individual cells were exported to Excel.

The geometric mean PE values of the respective calibration bead subsets were exported and used to calculate m (slope) and b (intercept) in linear regression (**Equation (1)**).

$$Log_{10}(PE_{Geomean} / bead) = m \times Log_{10}(\#PE / bead) + b \quad (1)$$

Because PE molecules were conjugated with anti-HA protein at a 1:1 ratio, this equation converted the PE readout of cells directly to the number of OXTRs/cell. A calibration curve was established to translate the PE fluorescence to the number of PE molecules.

PE background fluorescence (PE-FMO) was subtracted from the PE fluorescence of PE-stained samples, using a weighted integral approach (**Equation (2)**).

$$PE_{\text{absolute}} = PE_{\text{stained}} \times \left(1 - \frac{\left(\sum PE_{\text{background}}\right)/(n_{PE-FMO})}{\left(\sum PE_{\text{stained}}\right)/(n_{\text{stained}})}\right. \quad (2)$$

$PE_{absolute}$ is the number of receptors per cell obtained after subtracting $PE_{background}$, which was obtained from PE-FMO samples. $PE_{stained}$ is the unsubtracted receptor level measured in a PE-stained sample. $n_{stained}$ and $n_{PE\text{-}FMO}$ are the cell numbers collected from PE-stained and PE-FMO samples, respectively.

7.1.5. HEK293T western blotting

Twenty-four hours after transfection, cells were washed once with cold Hank's Buffered Saline Solution (Gibco) and then scraped directly into cold RIPA lysis buffer (Sigma) containing 1X Halt protease and phosphatase inhibitors (Thermo Scientific) and 100 g/mL

PMSF. Cells were lysed with 0.1-mm glass beads in a bullet blender (Stellar Scientific) for 2 min at speed 7. To remove insoluble material, the lysates were centrifuged at 10,000×*g* for 20 min at 4 °C. Lysates were quantified by bicinchoninic acid assay (Pierce) and mixed with Bolt™ LDS sample buffer with reducing agent (Novex, Thermo Fisher Scientific) before heating at 70 °C for 10 min. Samples were loaded (25 μg/well) onto 7.5% or 10% Mini-PROTEAN® TGX™ Precast Protein Gels (Bio-Rad) and run at 125 V in Tris-Glycine SDS running buffer (Bio-Rad). Gels were transferred to nitrocellulose membranes (0.45 μm, Bio-Rad) in Tris-Glycine transfer buffer (Bio-Rad) at 100 V for 90 min. Total protein was imaged by staining the nitrocellulose for 5 min with Revert™ 700 Total Protein Stain (Li-Cor). Blots were blocked with 5% milk in PBST (PBS + 0.075% Tween 20), incubated with rabbit anti-HA antibody (Cell Signaling; 1:1000 in 3% milk PBST) for 1 h at room temperature or overnight at 4 °C, washed three times 5 min, incubated with horseradish peroxidase-linked goat anti-rabbit secondary antibody (Cell Signaling; 1:10,000) for 1 h at room temperature, and then washed three times 5 min. The signal was developed with SuperSignal™ West Femto Maximum Sensitivity Substrate (Thermo Fisher Scientific) and imaged on a ChemiDoc™ MP Imaging System (Bio-Rad). Blots were analyzed with Image Lab (v 6.1.0) software (Bio-Rad). Band optical density for each sample was normalized to the total protein for that lane before normalizing to the WT sample. Values were imputed into GraphPad Prism (9.5.1) and compared by one-way ANOVA.

7.1.6. hTERT-HM GFP$^+$ sorting and western blotting

hTERT-HM cells were transfected as described above. Twenty-four hours after transfection, cells were lifted with TrypLE, pelleted at 1000×*g* at room temperature for 5 min, and then resuspended in an ice-cold solution of Hoescht 33342 for 10 min on ice. Cells were pelleted again at 1000×*g* at 4 °C for 5 min before resuspending in an ice-cold FACS buffer. Samples were sorted on a BD FACSAriaII into cold FACS. Samples were pelleted at 1000×*g* at 4 °C for 10 min. The pellet was resuspended in a RIPA lysis buffer (Sigma) containing 1X Halt protease and phosphatase inhibitors (Thermo Scientific) and 1 mM PMSF at a volume of 1 μL/1000 cells, and lysed by trituration. Samples were mixed with Bolt™ LDS sample buffer with reducing agent (Novex, Thermo Fisher Scientific) before heating at 70 °C for 10 min. Thirty microliters of each sample were loaded onto 4–12% Bis-Tris Bolt gel and run at 160 V for 1hr. The gel was transferred to PVDF at 100 V for 70 min. Blots were blocked with 5% milk in PBST (PBS + 0.075% Tween 20) overnight at 4 °C, incubated with rabbit anti-HA antibody (Cell Signaling; 1:1000 in 3% milk PBST) or rabbit anti-Histone H3 (Abcam; 1:3000) for 1 h at room temperature, washed three times 5 min, incubated with horseradish peroxidase-linked goat anti-rabbit secondary antibody (Cell Signaling; 1:10,000) for 1 h at room temperature, and then washed three times 5 min. The signal was developed with SuperSignal™ West Femto Maximum Sensitivity Substrate (Thermo Fisher Scientific) and imaged on a ChemiDoc™ MP Imaging System (Bio-Rad). Blots were analyzed with Image Lab (v 6.1.0) software (Bio-Rad). HA band optical density for each sample was normalized to the Histone H3 band intensity for that sample before normalizing to the WT sample on the gel. The Histone H3 was used, instead of the total protein, as a loading control because the OXTR protein was over-represented in the total protein in the sorted GFP-positive cells, thus using the total protein as a loading control in this context would have introduced a bias, as the overexpressed OXTR would skew the normalization. Values were imputed into GraphPad Prism (9.5.1) and compared by student's t-test.

7.1.7. Quantification and statistical analysis

Ensemble-averaged numbers of OXTR molecules in the whole cell and on the cell surface are presented as the number of receptors per cell (mean ± SEM). Statistical significance of differences was determined by two-sample *t*-test, Kruskal-Wallis ANOVA, ordinary one-way ANOVA, or Wilcoxon Signed-Rank test, as specified in the figure legends. Statistical tests were conducted in Originlab Pro or GraphPad Prism (9.5.1).

CRediT authorship contribution statement

Yingye Fang: Writing – review & editing, Writing – original draft, Visualization, Methodology, Investigation, Formal analysis, Data curation, Conceptualization. **Erin L. Reinl:** Writing – review & editing, Visualization, Data curation. **Audrey Liu:** Writing – review & editing, Data curation. **Trinidi D. Prochaska:** Writing – review & editing, Data curation. **Manasi Malik:** Writing – review & editing, Methodology. **Antonina I. Frolova:** Writing – review & editing, Supervision. **Sarah K. England:** Writing – review & editing, Supervision, Project administration, Investigation, Funding acquisition, Conceptualization. **Princess I. Imoukhuede:** Writing – review & editing, Supervision, Project administration, Investigation, Funding acquisition, Conceptualization.

Declaration of competing interest

The authors declare the following financial interests/personal relationships which may be considered as potential competing interests:

Princess Imoukhuede reports financial support was provided by Eunice Kennedy Shriver National Institute of Child Health and Human Development, 5R01HD096737-05 and the National Science Foundation, 2344705 Step 4. Accept the Agreement and pay ($2100 for open access). Sarah K. England reports financial support was provided by Eunice Kennedy Shriver National Institute of Child Health and Human Development. If there are other authors, they declare that they have no known competing financial interests or personal relationships that could have appeared to influence the work reported in this paper.

Acknowledgments

This material is based upon work supported by the National Institute of Child Health and Human Development (R01 HD096737 to

S.K.E. and P.I.I.) and the National Science Foundation. (Grant No. 1653925 to P.I.I.). The authors declare no competing financial interest. The authors express their appreciation to Dorjan Brinja and the Flow Cytometry Core in the Department of Pathology and Immunology at Washington University in St. Louis for their assistance in cell sorting. The authors thank the Genome Engineering and iPSC Center (GEiC) at Washington University in St. Louis for gRNA design and validation services. The authors are grateful to Deborah Frank and Andrew Kirsh for their rigorous and insightful review and editing of the manuscript.

Appendix A. Supplementary data

Supplementary data to this article can be found online at https://doi.org/10.1016/j.heliyon.2024.e25761.

References

[1] Y. Jin, D. Song, Y. Yan, Z. Quan, H. Qing, The role of oxytocin in Early-Life-Stress-Related neuropsychiatric disorders, Int. J. Mol. Sci. 24 (2023) 10430, https://doi.org/10.3390/IJMS241310430, 10430 24 (2023).
[2] M.G. Tesemma, D.A. Sori, D.H. Gemeda, High dose and low dose oxytocin regimens as determinants of successful labor induction: a multicenter comparative study, BMC Pregnancy Childbirth 20 (2020) 1–8, https://doi.org/10.1186/S12884-020-02938-4/TABLES/3.
[3] A.G. Cahill, B.M. Waterman, D.M. Stamilio, A.O. Odibo, J.E. Allsworth, B. Evanoff, G.A. Macones, Higher maximum doses of oxytocin are associated with an unacceptably high risk for uterine rupture in patients attempting vaginal birth after cesarean delivery, Am. J. Obstet. Gynecol. 199 (2008) 32.e1–32.e5, https://doi.org/10.1016/J.AJOG.2008.03.001.
[4] A.R. Fuchs, F. Fuchs, P. Husslein, M.S. Soloff, M.J. Fernström, Oxytocin receptors and human parturition: a dual role for oxytocin in the initiation of labor, Science 215 (1982) 1396–1398, https://doi.org/10.1126/SCIENCE.6278592, 1979.
[5] M. Maggi, P. Del Carlo, G. Fantoni, S. Giannini, C. Torrisi, D. Casparis, G. Massi, M. Serio, Human myometrium during pregnancy contains and responds to VI vasopressin receptors as well as oxytocin receptors, J. Clin. Endocrinol. Metab. 70 (1990) 1142–1154, https://doi.org/10.1210/JCEM-70-4-1142.
[6] L.B. King, H. Walum, K. Inoue, N.W. Eyrich, L.J. Young, Variation in the oxytocin receptor gene predicts brain region specific expression and social attachment, Biol. Psychiatr. 80 (2016) 160, https://doi.org/10.1016/J.BIOPSYCH.2015.12.008.
[7] R. Nissenson, G. Flouret, O. Hechter, Opposing effects of estradiol and progesterone on oxytocin receptors in rabbit uterus, Proc. Natl. Acad. Sci. USA 75 (1978) 2044–2048, https://doi.org/10.1073/PNAS.75.4.2044.
[8] M. Yoshida, Y. Takayanagi, K. Inoue, T. Kimura, L.J. Young, T. Onaka, K. Nishimori, Evidence that oxytocin exerts anxiolytic effects via oxytocin receptor expressed in serotonergic neurons in mice, J. Neurosci. 29 (2009) 2259–2271, https://doi.org/10.1523/JNEUROSCI.5593-08.2009.
[9] K.C. Leong, S. Cox, C. King, H. Becker, C.M. Reichel, Oxytocin and rodent models of addiction, Int. Rev. Neurobiol. 140 (2018) 201–247, https://doi.org/10.1016/BS.IRN.2018.07.007.
[10] M. Malik, Y. Fang, M. Wakle-Prabagaran, M. Roh, K. Prifti, A.I. Frolova, S.K. England, Pharmacological chaperones for the oxytocin receptor increase oxytocin responsiveness in myometrial cells, J. Biol. Chem. 298 (2022) 101646, https://doi.org/10.1016/j.jbc.2022.101646.
[11] M. Malik, M.D. Ward, Y. Fang, J.R. Porter, M.I. Zimmerman, T. Koelblen, M. Roh, A.I. Frolova, T.P. Burris, G.R. Bowman, P.I. Imoukhuede, S.K. England, Naturally Occurring Genetic Variants in the Oxytocin Receptor Alter Receptor Signaling Profiles, 2021, https://doi.org/10.1021/acsptsci.1c00095.
[12] Q. Chen, L.J. Miller, M. Dong, Role of N-linked glycosylation in biosynthesis, trafficking, and function of the human glucagon-like peptide 1 receptor, Am. J. Physiol. Endocrinol. Metab. 299 (2010), https://doi.org/10.1152/AJPENDO.00067.2010.
[13] Y. Fang, M. Malik, S.K. England, P.I. Imoukhuede, Absolute quantification of plasma membrane receptors via quantitative flow cytometry, Methods Mol. Biol. 2475 (2022) 61–77, https://doi.org/10.1007/978-1-0716-2217-9_4.
[14] E.L. Reinl, Z.A. Goodwin, N. Raghuraman, G.Y. Lee, E.Y. Jo, B.M. Gezahegn, M.K. Pillai, A.G. Cahill, C. de Guzman Strong, S.K. England, Novel oxytocin receptor variants in laboring women requiring high doses of oxytocin, Am. J. Obstet. Gynecol. 217 (2017), https://doi.org/10.1016/j.ajog.2017.04.036, 214.e1-214.e8.
[15] H.A. Frey, M.G. Tuuli, S.K. England, K.A. Roehl, A.O. Odibo, G.A. Macones, A.G. Cahill, Factors associated with higher oxytocin requirements in labor, J. Matern. Fetal Neonatal Med. 28 (2015) 1614–1619, https://doi.org/10.3109/14767058.2014.963046.
[16] S. Finley, P. Angelikopoulos, P. Koumoutsakos, A. Popel, Pharmacokinetics of anti-VEGF agent aflibercept in cancer predicted by data-driven, molecular-detailed model, CPT Pharmacometrics Syst. Pharmacol. 4 (2015) 641–649, https://doi.org/10.1002/psp4.12040.
[17] K.A. Norton, Z. Han, A.S. Popel, N.B. Pandey, Antiangiogenic cancer drug sunitinib exhibits unexpected proangiogenic effects on endothelial cells, OncoTargets Ther. 7 (2014) 1571–1582, https://doi.org/10.2147/OTT.S65055.
[18] D. Li, S.D. Finley, Integrative Biology the impact of tumor receptor heterogeneity on the response to anti-angiogenic cancer treatment, Integr. Biol. 10 (2018) 253–269, https://doi.org/10.1039/C8IB00019K.
[19] P.I. Imoukhuede, A.S. Popel, Quantitative fluorescent profiling of VEGFRs reveals tumor cell and endothelial cell heterogeneity in breast cancer xenografts, Cancer Med. 3 (2014) 225–244, https://doi.org/10.1002/cam4.188.
[20] S. Chen, T. Le, B.A.C. Harley, P.I. Imoukhuede, Characterizing glioblastoma heterogeneity via single-cell receptor quantification, Front. Bioeng. Biotechnol. 6 (2018) 92, https://doi.org/10.3389/fbioe.2018.00092.
[21] Y. Fang, P.I. Imoukhuede, Axl and vascular endothelial growth factor receptors exhibit variations in membrane localization and heterogeneity across monolayer and spheroid high-grade serous ovarian cancer models, GEN Biotechnology 2 (2023) 43–56, https://doi.org/10.1089/GENBIO.2022.0034.
[22] S. Chen, P.I. Imoukhuede, Single-cell receptor quantification of an in vitro coculture angiogenesis model reveals VEGFR, NRP1, Tie2, and PDGFR regulation and endothelial heterogeneity, Processes 7 (2019), https://doi.org/10.3390/pr7060356.
[23] S. Chen, X. Guo, O. Imarenezor, P.I. Imoukhuede, Quantification of VEGFRs, NRP1, and PDGFRs on endothelial cells and fibroblasts reveals serum, intra-family ligand, and cross-family ligand regulation, Cell. Mol. Bioeng. 8 (2015) 383–403, https://doi.org/10.1007/s12195-015-0411-x.
[24] P.I. Imoukhuede, A.O. Dokun, B.H. Annex, A.S. Popel, Endothelial cell-by-cell profiling reveals the temporal dynamics of VEGFR1 and VEGFR2 membrane localization after murine hindlimb ischemia, Am. J. Physiol. Heart Circ. Physiol. 304 (2013) 1085–1093, https://doi.org/10.1152/ajpheart.00514.2012.-VEGF.
[25] P.I. Imoukhuede, A.S. Popel, Quantification and cell-to-cell variation of vascular endothelial growth factor receptors, Exp. Cell Res. 317 (2011) 955–965, https://doi.org/10.1016/j.yexcr.2010.12.014.
[26] Y. Fang, L. Chen, P.I. Imoukhuede, Toward Blood-Based Precision Medicine: Identifying Age-sex-specific Vascular Biomarker Quantities on Circulating Vascular Cells, Cell Mol Bioeng, 2023, https://doi.org/10.1007/s12195-023-00771-1.
[27] J.C. Weddell, P.I. Imoukhuede, Quantitative characterization of cellular membrane-receptor heterogeneity through statistical and computational modeling, PLoS One 9 (2014), https://doi.org/10.1371/journal.pone.0097271.
[28] W.H. Tan, A.S. Popel, F. Mac Gabhann, Computational model of Gab1/2-dependent VEGFR2 pathway to Akt activation, PLoS One 8 (2013) e67438, https://doi.org/10.1371/journal.pone.0067438.
[29] L.W. Clegg, F. Mac Gabhann, Site-specific phosphorylation of VEGFR2 is mediated by receptor trafficking: insights from a computational model, PLoS Comput. Biol. 11 (2015) 1–36, https://doi.org/10.1371/journal.pcbi.1004158.
[30] S. Sarabipour, K. Ballmer-Hofer, K. Hristova, VEGFR-2 conformational switch in response to ligand binding, Elife 5 (2016), https://doi.org/10.7554/eLife.13876.

[31] M. Song, S.D. Finley, Mechanistic insight into activation of MAPK signaling by pro-angiogenic factors, BMC Syst. Biol. 12 (2018) 1–17, https://doi.org/10.1186/s12918-018-0668-5.
[32] M. Song, S.D. Finley, ERK and Akt Exhibit Distinct Signaling Responses Following Stimulation by Pro- Angiogenic Factors, 2020, pp. 1–19.
[33] K. Pierzynowska, L. Gaffke, M. Żabińska, Z. Cyske, E. Rintz, K. Wiśniewska, M. Podlacha, G. Węgrzyn, Roles of the oxytocin receptor (OXTR) in human diseases, Int. J. Mol. Sci. 24 (2023) 3887, https://doi.org/10.3390/IJMS24043887. Page 3887 24 (2023).
[34] S.S. Frehner, K.T. Dooley, M.C. Palumbo, A.L. Smith, M.M. Goodman, K.L. Bales, S.M. Freeman, Effect of sex and autism spectrum disorder on oxytocin receptor binding and mRNA expression in the dopaminergic pars compacta of the human substantia nigra, Phil. Trans. Biol. Sci. 377 (2022), https://doi.org/10.1098/RSTB.2021.0118.
[35] M. Trapecar, E. Wogram, D. Svoboda, C. Communal, A. Omer, T. Lungjangwa, P. Sphabmixay, J. Velazquez, K. Schneider, C.W. Wright, S. Mildrum, A. Hendricks, S. Levine, J. Muffat, M.J. Lee, D.A. Lauffenburger, D. Trumper, R. Jaenisch, L.G. Griffith, Human physiomimetic model integrating microphysiological systems of the gut, liver, and brain for studies of neurodegenerative diseases, Sci. Adv. 7 (2021), https://doi.org/10.1126/SCIADV.ABD1707/SUPPL_FILE/ABD1707_SM.PDF.
[36] D. Li, Y. Ji, C. Zhao, Y. Yao, A. Yang, H. Jin, Y. Chen, M. San, J. Zhang, M. Zhang, L. Zhang, X. Feng, Y. Zheng, OXTR overexpression leads to abnormal mammary gland development in mice, J. Endocrinol. 239 (2018) 121–136, https://doi.org/10.1530/JOE-18-0356.
[37] D. Li, M. San, J. Zhang, A. Yang, W. Xie, Y. Chen, X. Lu, Y. Zhang, M. Zhao, X. Feng, Y. Zheng, Oxytocin receptor induces mammary tumorigenesis through prolactin/p-STAT5 pathway, Cell Death Dis. 12 (2021) 1–13, https://doi.org/10.1038/s41419-021-03849-8, 6 12 (2021).
[38] J. Condon, S. Yin, B. Mayhew, R.A. Word, W.E. Wright, J.W. Shay, W.E. Rainey, Telomerase immortalization of human myometrial cells, Biol. Reprod. 67 (2002) 506–514, https://doi.org/10.1095/BIOLREPROD67.2.506.